Convection Patterns: Time Evolution of the Wave-Vector Field

M. S. Heutmaker, P. N. Fraenkel, and J. P. Gollub
Department of Physics, Haverford College, Haverford, Pennsylvania 19041, and Department of Physics, University of Pennsylvania, Philadelphia, Pennsylvania 19104
(Received 6 February 1985)

The evolution of Rayleigh-Bénard convection patterns has been studied quantitatively with use of digital image processing methods to measure the time dependence of the wave-vector field. The relative importance of wave-number variations, roll curvature, defects, and sidewalls was determined, with the Swift-Hohenberg model as a framework for analysis. Deviations from the model become pronounced for $(R - R_c)/R_c > 2$, where R_c is the critical Rayleigh number.

PACS numbers: 47.20.+m, 47.25.−c

In many nonlinear systems, a homogeneous state becomes unstable to spatially periodic perturbations when the critical value of a parameter is exceeded. Hydrodynamic instabilities and morphological instabilities of growing crystals are examples. Stability theory yields the onset and critical wave number of the instability, but does not generally give unique predictions for the form or evolution of the resulting patterns at a finite distance above the onset. A particularly challenging problem is that of the formation of Rayleigh-Bénard convection patterns in a large layer.[1-8] These are often textured structures containing defects; they cannot be described by a single wave number, but may be specified by a two-dimensional wave-vector field $\mathbf{q}(\mathbf{r})$ that contains the full information about orientations and spacings in the pattern.

We show in this paper that $\mathbf{q}(\mathbf{r})$ can be measured experimentally using digital image processing methods. We use this information, in conjunction with a two-dimensional model[8-10] for convective pattern evolution, to study various contributions to the dynamics, including defects, roll curvature, and the effects of boundaries. Model equations are useful in part because it is difficult to integrate the full hydrodynamic equations over the long time scales characterizing pattern evolution. Various models have been studied numerically[8,11] and analytically,[4,7,10] but none of them have yet been tested experimentally. The particular model we consider (due originally to Swift and Hohenberg[9]) is a simplification of the hydrodynamic equations having the following interesting property: a functional F of the dynamical fields decreases montonically, in analogy to the minimization of the free energy in equilibrium processes.

We find that the validity of the model depends strongly on the distance $\epsilon = (R - R_c)/R_c$ above the onset of convection. The experiments are consistent with the model provided that ϵ is neither too close to onset, nor larger than a cutoff $\epsilon_{max} \approx 2$. Using the model as a framework for analysis, we find that changes in the magnitude of the wave-vector field due to defect motion are particularly important, while roll curvature and lateral boundaries contribute much less to F.

The experiments were performed in a cylindrical convection cell of diameter $D = 86$ mm and depth $d = 3.0$ mm (aspect ratio $\Gamma = D/2d = 14.4$). The working fluid is water at 70 °C where its Prandtl number is 2.5, and the critical temperature difference ΔT_c is 0.720 °C. The horizontal thermal diffusion time τ_h based on the cell radius is 3.1 h. The structure of the convective flow is determined by the refraction of an expanded and collimated laser beam that enters the cell from above, traverses the fluid, reflects from the lower plate and impinges on a diffuse screen, where it is digitized (resolution of 320 pixels × 240 pixels × 8 bits) by use of Newvicon camera as a transducer. The apparatus will be described in detail elsewhere.[12] Digitized images are averaged to reduce noise, divided by a reference image (with no convection), and then contrast enhanced to reveal the weak convective structure.[2]

Figure 1 shows four contrast-enhanced images from a sequence at $\epsilon = 0.7$. Bright areas mark the cold (descending) fluid and dark areas mark the warm (ascending) fluid. In order to obtain patterns that evolve sub-

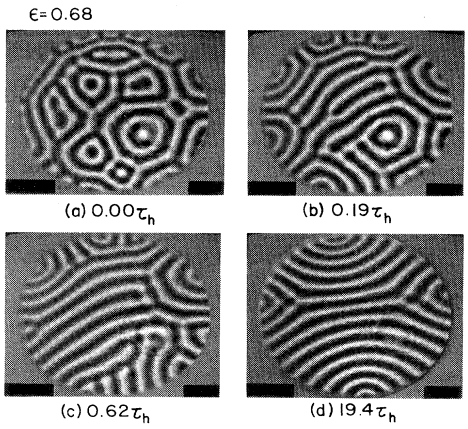

FIG. 1. Digitally enhanced images from a pattern evolution sequence at $\epsilon = (R - R_c)/R_c = 0.7$; time is given in units of the horizontal thermal diffusion time τ_h.

stantially, the system was prepared in a turbulent state, and then ϵ was reduced to 0.7. As time passes the initial cellular pattern quickly changes to bent convection rolls with many point defects (similar to dislocations and disclinations in solids) and line defects (similar to grain boundaries), as shown in Fig. 1(b). The defects are slowly expelled from the pattern until a final time-independent state is reached in which the rolls align nearly perpendicular to the sidewalls, and few defects remain. The evolution process is slow; major changes occur within the first horizontal thermal diffusion time, but at least 10–20 thermal diffusion times are required for the pattern to stabilize.

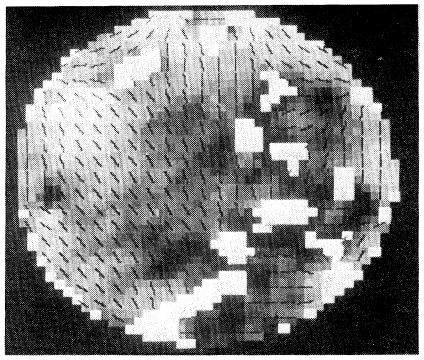

FIG. 2. Wave-vector field $\mathbf{q}(\mathbf{r})$ on a grid of points for the pattern of Fig. 1(c), as determined by digital image analysis. The background intensity is coded in proportion to the wave number, while the line segments indicate the orientation of the wave vector. The white excluded areas with no orientation lines contain defects.

In order to study the pattern evolution quantitatively, we obtain the wave-vector field $\mathbf{q}(\mathbf{r})$ by digital analysis of the images. The role boundaries are first found by following contours of maximum or minimum intensity. A grid of evenly spaced points is then superimposed over the pattern. The local roll orientation and spacing are interpolated at each grid point from the nearby roll boundaries in order to find the local orientation and magnitude of the wave vector. Small areas near defects are excluded from this calculation since the wave vector is undefined there. Figure 2 shows the result of this calculation for the pattern of Fig. 1(c). The background intensity is coded in proportion to the wave number $q(\mathbf{r}) = |\mathbf{q}(\mathbf{r})|$, while the line segments indicate the orientation of $\mathbf{q}(\mathbf{r})$. The white excluded areas mark the locations of defects.

Measurement of the wave-vector field allows us to use the Swift-Hohenberg model as a framework for analysis, and to estimate its range of validity. This model is an evaluation equation for a real order-parameter field $\psi(x,y,t)$ that is proportional to the vertical velocity and temperature at a fixed height in the fluid layer. One of the most important properties of this model is that it is variational; as ψ evolves a Lyapunov functional F decreases monotonically:

$$F = \int d^2r \{ \tfrac{1}{2}\epsilon^2 - \tfrac{1}{2}\epsilon\psi^2 + \tfrac{1}{2}(\xi_0^2/4q_0^2)[(\nabla^2 + q_0^2)\psi]^2 + \tfrac{1}{4}g\psi^4 \}.$$

In this equation ξ_0 is a coherence length scale, q_0 is a reference wave number, and g is a coupling constant of order unity. On the sidewalls of the cell, ψ and its normal derivative vanish. Far from the sidewalls, the model favors a static pattern of straight rolls with wave number $q = q_0$. Numerical simulations[8] and analysis[9] suggest that the model is appropriate for small ϵ.

Near onset in a laterally large layer ($\epsilon^{1/2}\Gamma \gg 1$), Cross showed that one can separate the contribution to F due to roll distortion in the bulk of the cell from that due to the suppression of convection near the sidewalls.[10] The bulk contribution can be written approximately[13] in terms of the wave-vector field $\mathbf{q}(\mathbf{r})$ of the pattern:

$$F_B \cong \epsilon\xi_0^2 \int d^2r \{ (q - q_0)^2 + (1/4q_0^2)(\nabla \cdot \mathbf{q})^2 \}.$$

This integral depends on two quantities: the square of the wave-number deviations $(q - q_0)^2$ and the square of the wave-vector divergence $(\nabla \cdot \mathbf{q})^2/q_0^2$, which is predominantly a measure of roll curvature. The sidewall contribution is minimized when the rolls are aligned perpendicular to the sidewall:

$$F_S = \tfrac{2}{3}\sqrt{2}\epsilon^{3/2}\xi_0 \oint [(\mathbf{q}\cdot\hat{\mathbf{s}})/q]\, dl,$$

where $\hat{\mathbf{s}}$ is a unit vector normal to the sidewall and the integral is taken around the cell boundary.

The amplitude of convection is suppressed near defects in the pattern, and this results in further contributions to F, which may be approximated as

$$F_D = \tfrac{1}{2}\epsilon^2 N_D \pi r_c^2,$$

where N_D is the number of point defects (disclinations) in the pattern and r_c is the radius over which ψ is suppressed. We assume that $\xi < r_c < 2\xi$, where the coherence length ξ is $\xi_0\epsilon^{-1/2}$, and $\xi_0 = 0.385d$. Further theoretical work is required to specify it more precisely. The sum of all these contributions $F = F_B + F_S + F_D$ is predicted to decrease monotonically during pattern evolution.

For the reference wave number q_0, we use the experimentally measured wave number selected by a pattern of straight rolls.[14] This quantity decreases with increasing ϵ, similar to the trend exhibited by the mean wave number in our textured stable patterns.

Figure 3(a) shows the results of our experimental measurement of the two parts of F_B for the evolution sequence of Fig. 1, with $\epsilon = 0.7$. The spatial averages

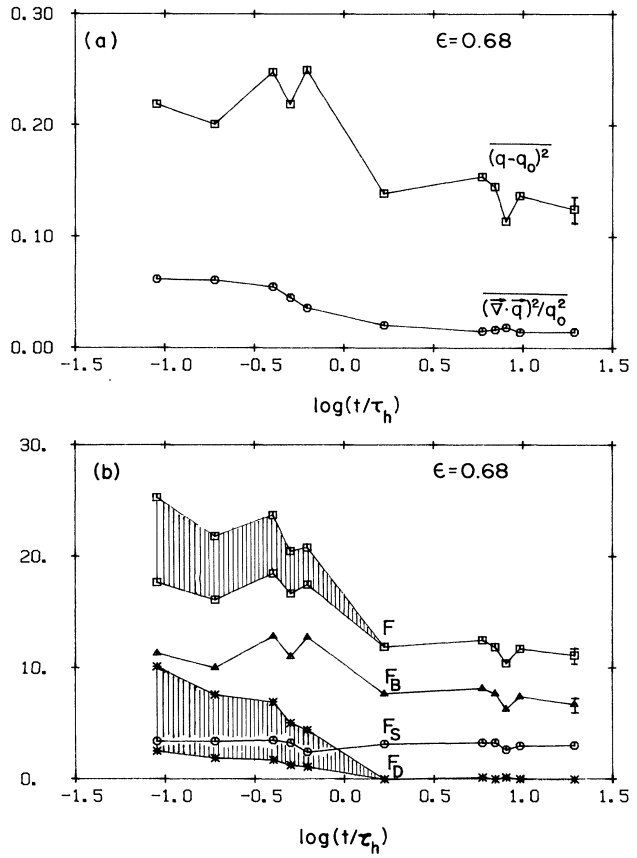

FIG. 3. (a) Spatial averages of the wave-number deviations $(q-q_0)^2$ and wave-vector divergence $(\nabla\cdot\mathbf{q})^2/q_0^2$ vs time (logarithmically) at $\epsilon=0.7$. (b) Total Lyapunov functional F and the bulk, defect, and sidewall contributions vs time (see text).

of $(q-q_0)^2$ and $(\nabla\cdot\mathbf{q})^2/q_0^2$ are shown as a function of $\log(t/\tau_h)$. (Lengths are measured in units of the cell depth.) We find that the wave-vector divergence decreases monotonically as the roll pattern becomes straighter, but the wave-number deviation is much larger and fluctuates significantly as defects move.

The total F and various contributions[13] to it are shown in Fig. 3(b). The sum is dominated by the bulk and defect terms F_B and F_D, while F_S is much smaller, and nearly constant. To determine the possible range of F_D, we assume that the effective core size is in the range $\xi < r_c < 2\xi$. (It would be better to measure the amplitude suppression directly to determine F_D, but the shadowgraph images are not sensitive to the suppression.) The total F is consistent with a monotonic decline, but the uncertainty is large because of the relatively large range for F_D.

We have performed this analysis on many other patterns both closer to and farther from onset. For small ϵ (<0.3), variations in F_B are small, and the decline of F_D as defects are eliminated causes the only significant change in the total. At long times (up to about $50\tau_h$) any variation in F is below our experimental resolution (about 10%), but the patterns are noticeably time dependent,[15] substantially so for $\epsilon\approx 0.1$. Therefore it is possible that the dynamics are not relaxational (monotonic) very close to onset. However, the evolution of F is qualitatively similar to that observed at $\epsilon=0.7$ up to $\epsilon\approx 2$. Thus we conclude that the minimization of F is consistent with our data over a range $\epsilon_{min}<\epsilon<\epsilon_{max}$, where $\epsilon_{min}\approx 0.3$ and $\epsilon_{max}\approx 2$.

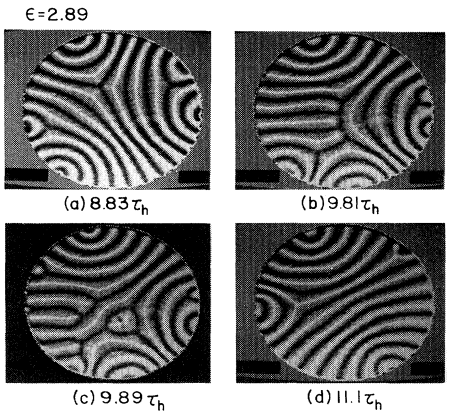

FIG. 4. Digitally enhanced images showing spontaneous defect nucleation at $\epsilon=2.9$.

For $\epsilon>\epsilon_{max}$, on the other hand, defects nucleate spontaneously as shown in Fig. 4, causing large nonmonotonic variations in F (Fig. 5). A large increase in F_B, due primarily to substantial wave-number variations, occurs when new defects enter the pattern. These major pattern changes seem to be precipitated by the climbing of newly created dislocations into regions of large roll spacing near defects in the bulk of the cell. We have observed the nucleation of these

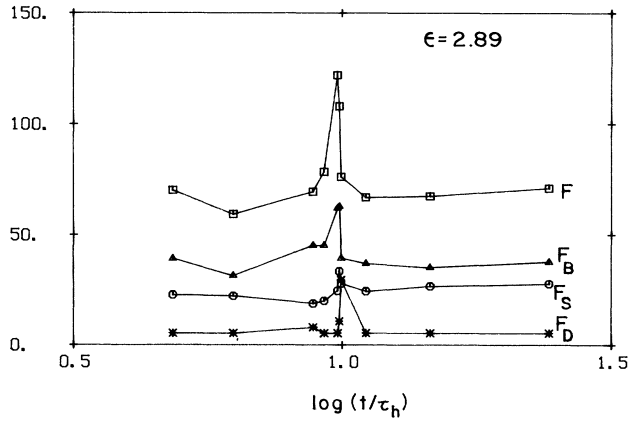

FIG. 5. Total Lyapunov functional F and bulk, defect, and sidewall contributions vs time at $\epsilon=2.9$. The nucleation of defects leads to nonmonotonic variations in F.

dislocations in each of three runs at $\epsilon = 2.9$.

The final-state patterns are clearly not unique (at any fixed ϵ), a result that was previously noted for rectangular[3] and smaller circular[2] cells. The various textured final patterns obtained from different initial conditions can have values of F differing by about 25%. We conclude that this functional must have many local minima.

Furthermore, we note significant qualitative differences in the way that the patterns adapt to the geometry[2] at small and large ϵ. For $\epsilon < 1$, grain boundaries are the dominant type of defect, while at higher ϵ disclinations are present. This is consistent with the different ϵ dependence of the various contributions to F, as well as with the increase with ϵ of the size of the band of stable wave numbers.

In summary, measurement of the time-dependent wave-vector field provides a useful way to characterize pattern evolution quantitatively. This can be accomplished by digital image analysis for evolving convection patterns. The Swift-Hohenberg model provides a framework for estimating the relative importance of defects, roll curvature, and wave-number variations. The largest changes in the Lyapunov functional F arise from wave-number variations associated with defect motion, while roll curvature and boundary effects are much smaller. Deviations from the model become pronounced above $\epsilon \approx 2$, though it is useful for a significant range of ϵ. A better understanding of point defects would allow a more precise comparison between theory and experiment. It would be desirable to test other models, some of which include nonrelaxational effects, and to investigate the effect of changing the Prandtl number.

This work was supported by the National Science Foundation through Grant No. MEA-8310933. We appreciate helpful discussions with G. Ahlers, M. Cross, and P. Hohenberg. One of us (J.P.G.) acknowledges the support of a Guggenheim fellowship.

[1]V. Croquette, M. Mory, and F. Schosseler, J. Phys. (Paris) **44**, 293 (1983).

[2]V. Steinberg, G. Ahlers, and D. S. Cannell, to be published. These authors also used digital image processing methods.

[3]J. P. Gollub, J. F. Steinman, and A. R. McCarriar, J. Fluid Mech. **125**, 259 (1982); J. P. Gollub and A. R. McCarriar, Phys. Rev. A **26**, 3470 (1982).

[4]M. C. Cross and A. C. Newell, Physica (Utrecht) **10D**, 299 (1984).

[5]M. C. Cross, P. G. Daniels, P. C. Hohenberg, and E. D. Siggia, J. Fluid Mech. **127**, 155 (1983).

[6]Y. Pomeau and P. Manneville, J. Phys. (Paris) **42**, 1067 (1981).

[7]P. Manneville, J. Phys. (Paris), Lett. **44**, L903 (1983).

[8]H. S. Greenside and W. M. Coughran, Jr., Phys. Rev. A **30**, 398 (1984).

[9]J. Swift and P. C. Hohenberg, Phys. Rev. A **15**, 319 (1977).

[10]M. C. Cross, Phys. Rev. A **25**, 1065 (1982).

[11]A. Zippelius and E. D. Siggia, Phys. Fluids **26**, 2905 (1983).

[12]M. S. Heutmaker and J. P. Gollub, to be published.

[13]The expression for F_B has been simplified for purposes of presentation. The actual equation we use to determine F_B has a small additional contribution. We also include a small term F_{GB} due to grain boundaries in the experimental determination of F [Figs. 3(b) and 5].

[14]A. Pocheau and V. Croquette, J. Phys. (Paris) **45**, 35 (1984).

[15]Persistent time dependence over even longer times has been convincingly demonstrated by G. Ahlers, D. S. Cannell, and V. Steinberg, following Letter [Phys. Rev. Lett. **54**, 1373 (1985)].

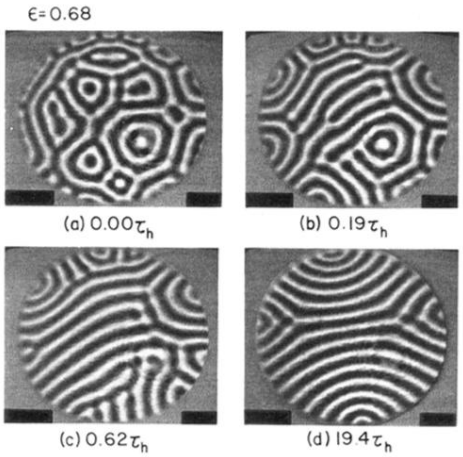

FIG. 1. Digitally enhanced images from a pattern evolution sequence at $\epsilon = (R - R_c)/R_c = 0.7$; time is given in units of the horizontal thermal diffusion time τ_h.

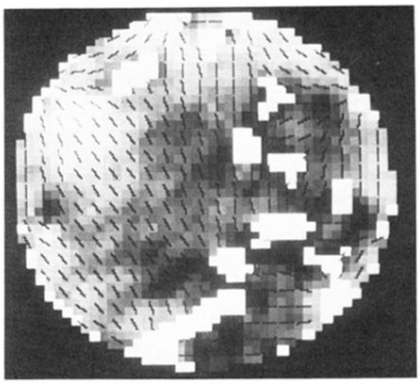

FIG. 2. Wave-vector field $\mathbf{q}(\mathbf{r})$ on a grid of points for the pattern of Fig. 1(c), as determined by digital image analysis. The background intensity is coded in proportion to the wave number, while the line segments indicate the orientation of the wave vector. The white excluded areas with no orientation lines contain defects.

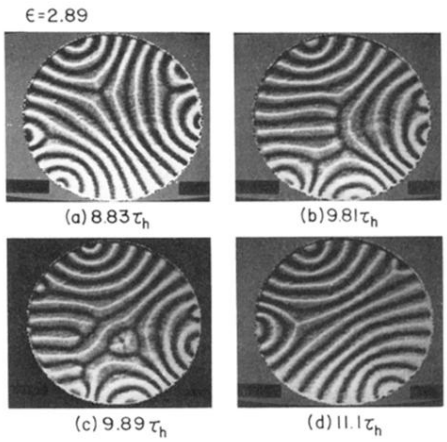

FIG. 4. Digitally enhanced images showing spontaneous defect nucleation at $\epsilon = 2.9$.